Surface Modifications for Greater Cycle Life and Energy Density in Lithium-Ion Batteries

by
Tucker M. Holstun

A THESIS

submitted to

Oregon State University

Honors College

in partial fulfillment of
the requirements for the
degree of

Honors Baccalaureate of Science in Chemical Engineering
(Honors Scholar)

Presented May 27, 2020
Commencement June 2021

AN ABSTRACT OF THE THESIS OF

Tucker Holstun for the degree of <u>Honors Baccalaureate of in Chemical Engineering</u> presented on May 27, 2021. Title: <u>Surface Modifications for Greater Cycle Life and Energy Density in Lithium-Ion Batteries</u>.

Abstract approved:_____

Zhenxing Feng

Significant challenges remain before lithium-ion batteries can support the decarbonization of the transportation and power sectors required to avert catastrophic climate change. The energy density of these batteries must be increased, while decreasing the price, and maintaining or increasing their lifespan. To improve the practical energy density of existing materials, more lithium must be extracted from the cathode upon charge. However, this additional lithium extraction requires an increased charging voltage and shortens battery cycling life. Previous theoretical work has predicted that complex oxides such as Li_2SrSiO_4 have promise as cathode coatings to extend cycle life under high voltage (e.g., 4.5 V versus lithium metal) operation. In this work, a dual sol-gel coating of Li_2SrSiO_4 and Al_2O_3 at the optimal thickness on $LiCoO_2$ has been shown to allow for charging to a greater cut-off voltage of 4.5V to access a greater gravimetric capacity of ~185 mAh/g. This greater stability at high cut-off voltages persists through high-rate cycling and maintains a good cycling life. Meanwhile, Li_2SrSiO_4 on its own failed to allow for stable cycling of $LiCoO_2$ at a higher voltage. The mechanism by which this coating scheme works was probed with several X-ray characterizations including X-ray absorption spectroscopy, and X-ray fluorescence and ptychography imaging to gather insight for work on even more effective ceramic cathode coatings in the future.

Key Words: Battery, Cathode, Lithium-ion, Surface Characterization, Electrochemistry

Corresponding e-mail address: holstunt@oregonstate.edu

Surface Modifications for Greater Cycle Life and Energy Density in
Lithium-Ion Batteries

by
Tucker M. Holstun

A THESIS

submitted to

Oregon State University

Honors College

in partial fulfillment of
the requirements for the
degree of

Honors Baccalaureate of Science in Chemical Engineering
(Honors Scholar)

Presented May 27, 2021
Commencement June 2021

<u>Honors Baccalaureate of Science in Chemical Engineering</u> project of Tucker Holstun presented on May 27, 2021.

APPROVED:

_____

Zhenxing Feng, Mentor, representing Department of Chemical Engineering

_____

Kelsey Stoerzinger, Committee Member, representing Department of Chemical Engineering

_____

Willie Rochefort, Committee Member, representing Department of Chemical Engineering

_____

Toni Doolen, Dean, Oregon State University Honors College

I understand that my project will become part of the permanent collection of Oregon State University, Honors College. My signature below authorizes release of my project to any reader upon request.

_____

Tucker M. Holstun, Author

Acknowledgements

I would like to thank Dr. Zhenxing Feng and Marcos Lucero for their incredibly generous support throughout this project. Dr. Feng provided significant and excellent support as a mentor, both in terms of consultation for data analysis and experimental design, but also as a guide for my professional development. Marcos Lucero contributed significantly both to the material characterization detailed in this work, but also in terms of advice and shared experience that were instrumental to my own contributions. Characterizations and help provided by Feng group members and collaborators (Maoyu Wang, Dr. Alpha R. N'Diaye, Dr. Junjing Deng, and Ryan Faase) were also critical to the interpretation of our electrochemical results. Additionally, the internship made possible by the Pete and Rosalie Johnson Foundation in the summer of 2018 allowed me to dedicate the time and resources needed to embark on a large research project. I would also like to thank Dr. Skip Rochefort and Dr. Kelsey Stoerzinger for sitting on my committee and, along with Dr. Trevor Carlisle, for their help during the graduate school application and decision process.

Table of Contents

1. Introduction

1.1 History and Context

The threat of catastrophic climate change demands appropriate action to minimize humanitarian harm and damage to the earth's ecosystems. Recent climate modelling suggests that we have only the next few decades to bring our greenhouse gas emissions to near zero to avoid greater than 2°C of average warming, the internationally agreed upon limit[1]. To achieve deep emissions cuts, every major sector of the economy must be rapidly decarbonized, meaning that power and heating in all parts of the economy must be provided from electricity derived from renewable energy sources, rather than fossil fuels. In the push to cut emissions as quickly as possible, transportation and grid-scale storage of renewables are seen as plausible targets for the direct substitution of fossil fuels by energy storage in batteries[2]. However, due to the low energy and power density of existing battery systems, the advent of practical electric vehicles and electrochemical grid storage did not come until the invention and mass production of the lithium-ion battery[3].
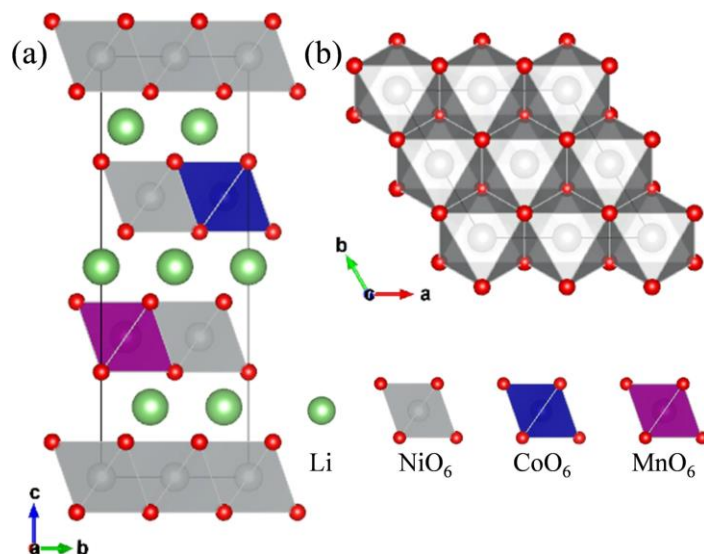
Figure 1: The crystal structure of layered cathode compounds showing lithium and transition metal layers from the a) side and b) top. The composition depicted is NMC811. From Lim et. al.[12].

Based on earlier work by Stanley Whittingham on layered $LiTiS_2$ as an electrode material, John B. Goodenough discovered the potential of higher voltage, structurally analogous $LiCoO_2$ (LCO) as a ~4V cathode material in 1979[4,5] (**Figure 1**). Paired with a lithium metal anode, these batteries constituted an extremely energy dense rechargeable battery. However, the lithium anodes used in early commercial cells were too dangerous to allow for widescale use. In 1985, Akira Yoshino assembled the first prototype lithium-ion battery with a $LiCoO_2$ cathode and a graphitic carbon

anode[6]. During charge, lithium ions were driven from the lithium layer in the metal oxide framework of a micron-sized cathode particle, as initiated by the oxidation of the transition metal from 3^+ to 4^+ by an electric current. They then travel through an electrolyte of $LiPF_6$ dissolved in an organic solvent, and into the layers between the sheets of carbon in micron-sized graphite on the anode side where electrons are being driven. Upon discharge, the lithium ions return from the anode to the cathode and "intercalate" back into its crystal structure as the electrons travel around through the circuit. Graphite proved to be much safer than using lithium metal as an anode, allowing for commercialization and subsequently the possibility of portable electronics such as cell phones and laptops with useful battery life. In the three decades since, a great deal of research has gone into reducing the price of these batteries, while increasing the energy density of this common architecture.

As of the publication of this work in 2021, the current price of a lithium-ion battery has fallen to nearly approximately \$100/kWh and the practical energy density of such cells can reach as high as ~275 Wh/kg[7]. This has allowed for the proliferation of lithium-ion batteries into both a rapidly growing number of electric vehicles, and the first grid-scale batteries for energy leveling[8]. However, significant challenges remain before lithium-ion batteries can help to electrify all ground transportation, let alone grid-scale storage. First, the energy density of current lithium-ion batteries is barely sufficient to allow a passenger vehicle to drive ~300 miles on a single charge and will need to be increased to make wide-spread electric heavy-duty vehicles practical. Additionally, the cost of these batteries is still not yet low enough for most people to be able to afford an electric vehicle, or to allow for a stable electrical grid with renewables and batteries alone[9]. Complicating both factors is the fact that only rare and expensive cobalt has sufficient octahedral ligand field stabilization energies to allow for stable cycling, while nickel is the only element that can do so with other dopants present[10]. As such, there is a drive to both increase the useful lifespan of such batteries, while reducing cost and increasing energy density, leading to research on protective cathode particle surface modifications and metallic dopants to reduce cobalt content in favor of nickel[11].

The term "lithium-ion battery" in modern usage obscures the very different compositions that can be labelled under this term. While the graphite anode and electrolyte composition are almost

universal across different cell formats and applications, the transition metal composition of the cathode can vary to a great degree. For example, while transition metal oxides of the structure originally discovered with $LiCoO_2$ are used in the cathodes of most cells currently being produced, the polyanionic $LiFePO_4$ has also grown in popularity[8]. However, for the purposes of this work on cathode surface modifications, only these layered species are of interest. This is because $LiFePO_4$ already achieves excellent cycle life at very near its theoretical, although limited, energy density[13]. Indeed, the advancement of electric vehicles was only made possible by the discovery that a solid solution of nickel, cobalt, manganese and/or aluminum can allow for cobalt substitution in a layered cathode material, reducing cost[14]. Paired with the alarming rarity, geographic restrictions, and human rights violations associated with some cobalt mining, there is a strong incentive for industry to replace cobalt to whatever degree possible[15]. This has resulted in a proliferation of the $LiNi_{1-x}Mn_xCo_yO_2$ (NMC) and $LiNi_{1-x}Co_xAl_yO_2$ (NCA) cathode classes to achieve acceptable cycling life with greater nickel content. The industry has pushed to NMC111, NMC532, NMC622 and eventually NMC811, where the numbers indicate the atomic fraction of each metal in the transition metal layer (i.e., NMC811 – $LiNi_{0.8}Mn_{0.1}Co_{0.1}O_2$). Despite the change in composition, the electrochemical window of these layered nickel-cobalt compounds remains remarkably similar, with most lithium extraction from the lattice occurring from 3.5V to 4.2V, leading to the ease of iterative cathode chemistry changes in products. The continual increase in the concentration of nickel has increased energy density and decreased cost but has worsened cathode-driven degradation mechanisms, making the complete elimination of cobalt impractical thus far [16].

Most current research on lithium-ion batteries for near-term applications focuses on the cathode material, rather than the electrolyte or anode. This is for several reasons: the potential material cost savings, the limitations of practical electrolytes and anode materials, and the potential for energy density improvement. Because the cathode is by far the most expensive component due to its cobalt and nickel content, there is the most incentive to change its composition or reduce the required amount for a given energy content[17]. The electrolyte and anode materials are also harder to modify without changes to the battery's operation. For example, many researchers are attempting to replace graphite anodes with very thin lithium metal anodes or silicon to increase energy density dramatically without the safety pitfalls of the thick lithium used in early research[18]. However, this presents very difficult cycle life issues which are unlikely to be overcome soon. Meanwhile,

graphite is cheap, operated to near its theoretical limit, and has a greater specific capacity than existing cathodes already. Additionally, the significant energy density gains that might still be extracted from layered cathode materials will come at the expense of accelerated degradation mechanisms at the cathode[19]. Taken together, these considerations mean that until a true electrolyte or anode material breakthrough is made, all foreseeable energy density gains and material cost savings will occur at the cathode side. As such, research to stabilize more energy dense cathode materials in the presence of existing electrolyte and anode formulations is likely to be useful for many years to come.

1.2 Degradation Mechanisms of Lithium-Ion Batteries

The degradation mechanisms of batteries using layered, transition metal oxides as their cathode vary in their severity but are the same across differing transition metal compositions. These mechanisms can be split into two general categories: bulk and surface.

1.2.1 Bulk Degradation

Bulk degradation mechanisms arise out of the electrostatic changes that occurs when lithium is removed from layered materials. Upon the removal of about half of the lithium from the lithium layer, the spacing between layers begins to contract noticeably[20]. First, this continuously increases the activation barrier for lithium migration, limiting high-rate applications. Upon further delithiation, the strain imposed by the shifting layered can cause phase transitions resulting from stacking rearrangements in the O-M-O network. These changes between stacking arrangements impart large, anisotropic volume changes on the cathode particles which can cause cracking at grain boundaries, and even cause phase transformations to spinel structures in the bulk of particles[21] (**Figure 2**). Because the contraction of the lithium layer is a function purely of the reduced Van der Waals repulsions, there are only two ways to prevent bulk degradation modes in layered materials: 1) suppressing phase transitions upon lithium layer collapse, which the short-range ordering effects in NMCs have already achieved to allow an additional ~30% lithium removal, or 2) pinning the lithium layers open via surface modifications. The changes that occur upon partial delithiation have limited the practical capacity of $LiCoO_2$ to ~140 mAh/g and NMC811to ~180 mAh/g, rather than their theoretical capacity of ~270 mAh/g upon complete delithiation[12,16,21].
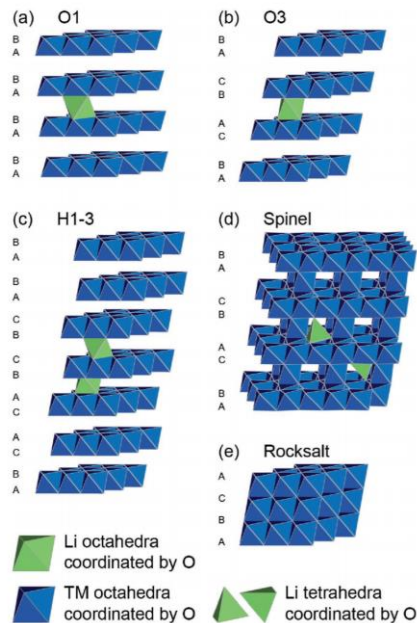
Figure 2: a-c) Different O-M-O ordering structures that arise upon material delithiation. d) spinel structure arising from migration of transition metals to lithium layers and forcing of lithium to tetrahedral sites. e) transition metal rocksalt with little to no lithium content and diffusion. From Radin et. al.[39].

1.2.2 Surface Degradation

As with bulk degradation, surface changes occur with greater severity at higher voltages, especially above the typical cut-off of 4.2 V[22]. The increased oxidation state of the cobalt or nickel upon charging to a higher voltage makes it more and more likely that the alkyl carbonate solvents in the electrolyte will be oxidized at the surface of the delithiated cathode particle. Not only does this cause a loss of oxygen from the cathode, densification of the surface, and an undesired rocksalt surface layer (i.e. Co_xO_y/NiO)[23], it also consumes electrolyte and creates H_2O. This water then partakes in many side reactions, the worst of which being reaction with $LiPF_6$ to form reactive hydrofluoric acid (HF)[24]. This HF can then corrode the cathode surface, which generates more H_2O, which continues a cycle of degradation that can continue until the entire surface of the cathode particle is composed of electrochemically inactive and impeding phases. In some cases, cobalt can even be leached from the particle[25]. Along with the Li_2CO_3, LiOH, and LiF that can form from lithium ions reacting with electrolyte side reaction products or exposure to air during manufacturing[26], the degraded surface phases constitute what is known as the cathode-electrolyte interface (CEI). This interface slows further reactions somewhat, but increases the charge transfer resistance, decreasing the capacity which the cathode can deliver. While a similar solid electrolyte

interface (SEI) forms at the anode, it does so without the consumption of active graphite or run-away reactions that continually thicken the film [27]. Without modifications to the composition of electrolyte formulations, it is therefore of critical interest to protect the surface of delithiated cathode particles from direct contact with the electrolyte.

1.3 Ceramic Cathode Coatings

The addition of thin, conformal ceramic coatings to the surface of layered cathodes has been shown many times to provide an improvement in the stability through repeated cycling to higher cut-off voltages[28]. Al_2O_3 is particularly well documented as an effective cathode coating on both LCO and NMC/NCA chemistries, although other simple metallic oxides are used such as ZrO_2 and TiO_2[29,30]. The effectiveness of this coating, and similar metal oxides is thought to be owed to its sacrificial reaction with corrosive HF, separation of the cathode surface from the organic electrolyte solvent and byproducts, prevention of cobalt leaching, and sufficient lithium-ion diffusivity[31]. By separating the destabilized cathode surface from the electrolyte entirely, the passivating function of the naturally forming CEI can be replaced without the loss of active cathode material. This has been shown to allow for the stable cycling of existing cathode materials to higher operating voltages (and therefore greater lithium extraction and energy density) which would cause rapid destruction of the cathode material and unacceptable cycling life in unmodified material.

Several methods have been developed for the application of cathode coatings. Most commonly, atomic layer deposition (ALD) has been utilized for depositing conformal, thin layers (~ 1 nm) of materials onto cathode particles[32]. Unfortunately, ALD is a process that has proven too slow, small-scale, and expensive due to the machinery and precursors required, making it likely uneconomic for application in wide-scale production of cathode material[33]. In addition, ALD so far can only handle relatively simple compounds (e.g., single, and binary elements). Materials with complex compositions, meaning more than one constituent metal, are hard to synthesize by ALD, greatly restricting the space of available and effective coating materials.

Previously, our group has demonstrated a similar benefit of coating Al_2O_3 to the surface of $LiCoO_2$ using a much more industrially feasible sol-gel technique[34]. In sol-gel techniques, a metal alkoxide precursor is polymerized or colloidally suspended in solution and then heated until only the desired

metal oxide remains. Although sol-gel coating methods produce a less uniform film which must be made much thicker, on the order of 10-100 nm rather than ~1nm for ALD, the disadvantage in lithium diffusion across the coating is outweighed by the challenges and cost of ALD[33]. Furthermore, there is no such restriction on materials composition when using sol-gel, thus making it feasible to coat more complex, promising candidate materials onto the surface of cathode particles.

1.4 Theoretical Basis for New Coating Materials

Despite the beneficial effects of Al_2O_3 on the surface of cathodes, it is unlikely to be the best choice of coating material. Two remaining problems arise from the use of Al_2O_3 to protect the surface of $LiCoO_2$ particles, which is chosen here as a simpler case study than NMC. First, during the heating process of sol-gel techniques the Al_2O_3 is predicted to react with the cathode surface, forming a solid solution of $LiAlO_2$, Co_3O_4, and Li_2CoO_3 at the boundary, each of which theoretical calculations show are less effective at scavenging HF than Al_2O_3, thus leaving the $LiCoO_2$ less protected than it could be[35]. Indeed, it seems that $LiCoO_2$ reacts with HF more readily than the components of the resulting mixture, making the presence of bare patches which are possible with sol-gel techniques more problematic. Second Al_2O_3 is not a good lithium-ion conductor, only developing acceptable lithium diffusivity after the lithium doping that necessarily occurs upon cycling[36].

High-throughput screening of potential cathode coating materials performed by Aykol et al. attempted to determine potentially superior cathode coatings to Al_2O_3 based on high HF reactivity, low reaction potential with cathode materials, electrochemical stability, and low mineral cost. On these bases, they identified Li_2SrSiO_4 (LSSO) as a highly promising cathode coating. In fulfillment of all search criteria, its many Si-O bonds are likely to react with HF, it has low material cost, good electrochemical stability, positive reaction energy with layered cathode materials, and a high likelihood of good ion conduction due to its lithium content[35]. Therefore, in the first work contained here, LSSO was coated onto $LiCoO_2$ via a sol-gel coating to assess its feasibility as a cathode coating.

2. Methods

2.1 Cathode Coatings

$LiCoO_2$ cathode powder was coated using sol-gel methods based on previous work by our group and others. In all cases a sol-gel solution was prepared by the dissolution of a gelling agent composed of one of the required elements, and salts of the others, in the required stoichiometry. In the case of Al_2O_3, a sol-gel was created by adding aluminum isopropoxide to HPLC grade ethanol to form a 1M solution and heated and mixed until dissolved. Li_2SrSiO_4 was created by mixing $LiNO_3$, $Sr(NO_3)_2$ and tetraethyl orthosilicate (TEOS) into ethanol in stoichiometric quantities except in the case of lithium, for which a 10% excess was used to counter evaporative losses during heating. Samples of both coating types were heated in a furnace under air to 450 °C for 3 hours to drive off organics, and then to 600 °C for an additional 3 hours to obtain a coated product. A heating rate of 5°C/min was used for the first heating ramp to avoid excessive disturbance of the sample as the organics were driven off, while 10 °C/min was used for the second heating ramp and cooling. In the case of Li_4SiO_4, the same procedure was used as for Li_2SrSiO_4, but with more lithium to replace the strontium content. For samples which were dual-coated, a coated sample was retrieved from the furnace and a coating of another material was applied over the first coating just as it would be on its own (**Figure 3**). Samples utilized for the confirmation of desired phases on the surface of $LiCoO_2$ using XRD were coated via an identical procedure, but greater loadings of LSSO and Al_2O_3 precursors.
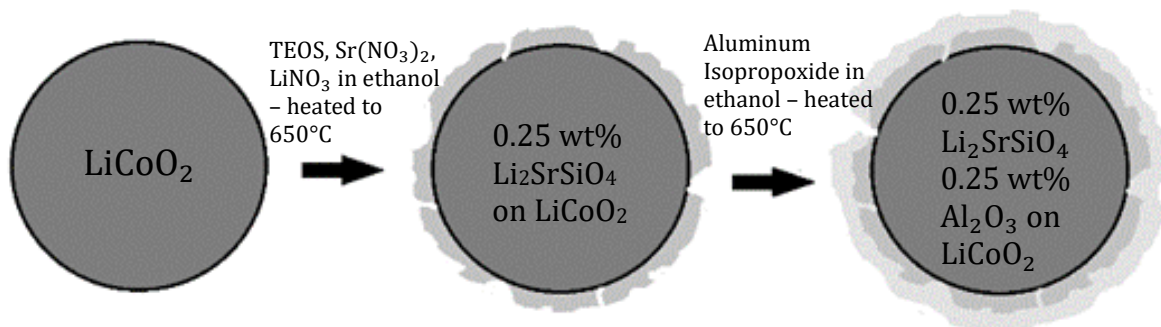

Figure 3: Schematic showing the application of coating layers in two sol-gel steps to the surface of a $LiCoO_2$ particle.

2.2 Powder X-Ray Diffraction

The phase of prepared materials was confirmed using p-XRD on a Bruker Diffractometer using a Copper Kα1 X-ray source on as-prepared powder. Samples were prepared by leveling powder in

the sample holder. VESTA was utilized along with cell parameters from previous publications of LSSO to generate the theoretical diffraction pattern for LSSO[37]

2.3 Electrode Fabrication:

Cathodes were created by mixing $LiCoO_2$ [MSE Supplies], C65 carbon black [MSE Supplies], and Polyvinylidene fluoride (PVDF) [Solvay]. An 8:1:1 mass ratio of these components was utilized. The cathode powder and carbon black were first ground by hand in a mortar and pestle for 30 minutes to coat the cathode powders with a conductive material. The material was then dried for 15 minutes at 60 °C to avoid moisture content in the slurry. 8 wt% PVDF in N-Methyl-2-pyrrolidone (NMP) was then added to this mixed powder and let to stir over night in a sealed vial to form a uniform slurry. This slurry was then cast onto aluminum such that its mass loading was 2-4 mg/cm^2. The slurry coated aluminum was then dried in a vacuum overnight at 70 °C overnight to evaporate the NMP and drive off contaminating moisture. The foils were then removed and ~1cm diameter circular cathodes were punched out and weighed to record their individual masses. The average mass of an uncoated aluminum punch of this size, 3.33 mg, was then subtracted from this mass to get the mass cathode loaded onto the foil, from which the cathode material loading could be determined from the mass fractions of cathode, black carbon and PVDF.

2.4 Test Cell Fabrication:

Coin cells were then assembled in an argon filled glovebox to prevent incorporation of air and moisture into the cells. Lithium foil was used as the anode instead of the graphite particles typically used in commercial cells, to avoid considerations such as lithium plating and the necessity of sufficient anode capacity. First, lithium foil was punched and then pressed manually into an anode cap for a CR2032 coil cell. Next, a punched-out, circular fiberglass separator of slightly greater diameter was placed over this lithium to prevent electrical contact with the cathode. 10 drops of 1M LiPF6 in 50/50 (v/v) ethylene carbonate (EC) and dimethyl carbonate (DMC) was then dispensed onto the separator to fully wet it, serving as the electrolyte of these cells. Next, the cathode of known areal loading was placed, active material down, onto this wetted separator. On top of the cathode, a steel separator and spring were placed which served to compress the working materials and ensure good contact between them. Finally, a cathode cap was placed over the full

stack and sealed to prevent exposure to air in an electric press. The full cells were then removed from the glovebox.

2.5 Electrochemical Tests

Cycling tests were performed on the assembled coin cells using a LANHE test rack and associated monitoring software. In all tests, cells were given 30 minutes to "rest", which allows for better electrolyte wetting of the cathodes and initial formation of electrolyte interfaces on the electrode materials. Cells with 2.0V to 3.0V open circuit voltages (as assembled) were accepted onto testing, while dysfunctional cells with lower-than-expected voltages were removed. In long duration cycling life tests, cells were then charged and discharged from 3.0V to 4.5V at a rate of 0.1C for two formation cycles (charging and discharging in 10 hours as defined by the active material mass and an assumed discharge capacity of 180 mAh/g). Subsequent cycles, up to 500 cycles in some cases, occurred over the same voltage window but at a higher 0.5C rate (charging and discharging in 2 hours). For high C-rate testing, after formation cells were charged and discharged at 0.5, 1, 2, 5 and 10 C-rates to determine the capacity and retention of the material under high-stresses.

Electrochemical impedance spectroscopy (EIS) was performed on both pristine cells and cells after 50 cycles at 0.5 C on a CHI760 potentiostat. EIS was conducted from $0.01 - 10^5$ Hz with an amplitude of 0.01V. Cyclic voltammetry (CV) scans were collected at a rate of 0.1 mV/s for three full charge and discharge cycles on assembled cells.

2.6 Cathode Particle Imaging

Cathode particle images and elemental mapping was obtained by X-ray ptychography and fluorescence imaging by Dr. Junjing Deng at Argonne National Laboratory.

2.7 X-ray Characterization

Hard X-ray absorption spectroscopy (hXAS) at the Co K-edge was performed at beamline 9BM of the Advanced Photon Source (APS) of Argonne National Laboratory (ANL). A cobalt metal reference was used as a standard to properly calibrate the energy. Both Co K-edge X-ray absorption near edge structure (XANES) and extended X-ray absorption fine structure (EXAFS) were

measured under fluorescence mode by a Vortex ME4 detector. Soft XAS (sXAS) was performed at Co L-edge and O K-edge using both fluorescence and electron yield modes at beamline 6.3.1 of Advanced Light Source (ALS) of Lawrence Berkeley National Laboratory (LBNL).

All XAS data analysis was performed with Athena software package to extract XANES and EXAFS. The EXAFS data were modelled using Artemis software package in k and R space in the ranges [3-13 Å-1] and [1-4.5 Å], respectively. XAS was performed and analyzed with insights from the previous experience and work of our group[38].

3. Results and Discussion

3.1 Powder X-ray Diffraction

Given that LSSO had never been synthesized on the convex hull of metal oxide particles, a 50 wt%, LSSO sol-gel coated sample was prepared to verify the existence of the correct phase. Once the presence of the desired phase had been confirmed, the retention of the $LiCoO_2$ phase after coating thin layers of both LSSO and Al_2O_3 onto the particles was confirmed by XRD.
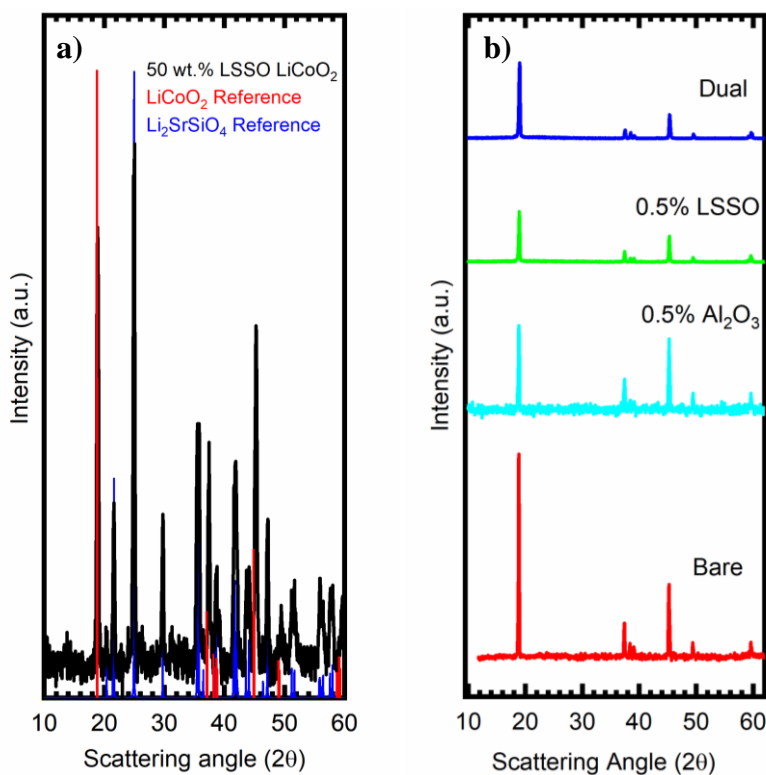

Figure 4: a) confirmation of the creation of desired Li_2SrSiO_4 phase on $LiCoO_2$ particles using a 50 wt% coating. b) confirmation of intact $LiCoO_2$ phase after coating.

As seen in **Figure 4**, both the presence of LSSO on the surface of the $LiCoO_2$ and the retention of the desired $LiCoO_2$ phase after coating were confirmed. In **Figure 4a**, the strong alignment of the measured XRD peaks on 50 wt% LSSO coated material to the theoretical peaks of the expected $LiCoO_2$ and LSSO phases can be observed. The lack of any clear peaks other than the theoretical diffraction pattern of either material suggests that minimal reaction occurs between the bulk $LiCoO_2$ and the LSSO at the synthesis temperature of 600°C. However, the difficulty of removing the significant background from the sample holder would make discerning impurity peaks from noise difficult. The diffraction pattern of 0.25 wt% LSSO and Al_2O_3 coated material in **Figure 4b** likewise showed that the crystal structure of the $LiCoO_2$ appeared unaltered by the application of these coatings. However, the signal from the coating layers was too weak in this material to resolve the pattern of Al_2O_3 or LSSO. The ability to synthesize Al_2O_3 on the surface of $LiCoO_2$ particles via the described sol-gel method was not explicitly confirmed here, as it is described in previous work by our group[34]. Additionally, reactions between the Li_2SrSiO_4 and Al_2O_3 at the boundary in mixed coatings, as will be discussed later, cannot be ruled out by XRD.

3.2 Narrowing Down Coating Schemes

Once the ability to coat LSSO onto the surface of $LiCoO_2$ as intended was verified, samples coated with practical thicknesses of LSSO and Al_2O_3 of 0.25, 0.5 and 1.0 wt%, as well as bare $LiCoO_2$ were compared in half-cell testing. Testing was performed at a moderate rate of 0.5 C, over a voltage window of 3.0V to a high voltage cut-off of 4.5V vs. Li/Li^+. Lithium foil was used as the anode of each "half-cell".
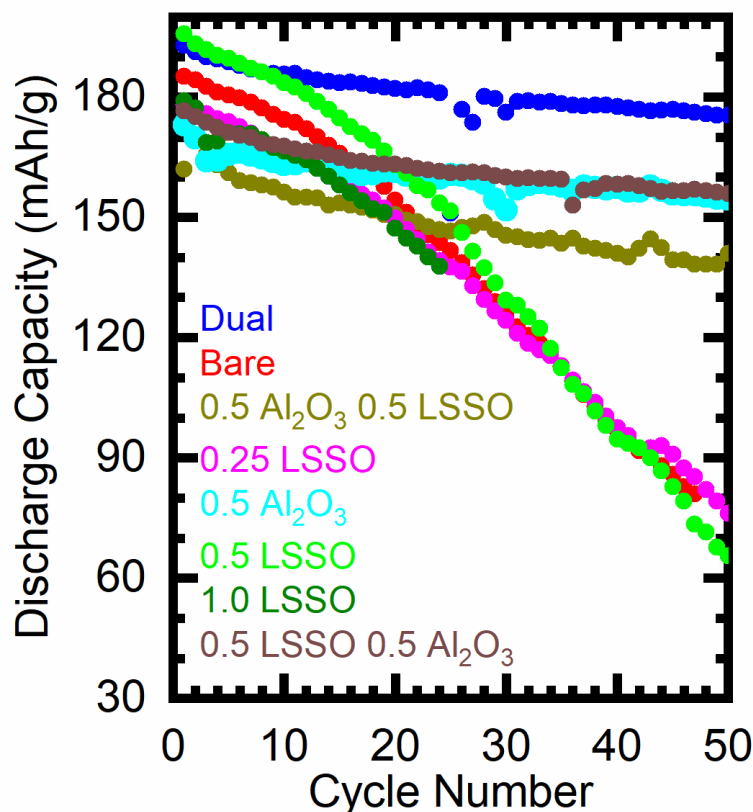
Figure 5: a) Comparison between half-cell cycling performance of different coating compositions, orientations, and thicknesses over 50 cycles at 3.0-4.5V and a 0.5 C-rate. In dual coatings the first denotes the inner layer – 0.25% LSSO is the inner layer in 0.25% LSSO 0.25% Al_2O_3.

In contrast with the predicted efficacy of LSSO as a coating for layered cathode materials, cycling data presented in **Figure 5** shows that LSSO coated material has very poor retention of capacity when charged to a higher upper cut-off voltage. Different coating loadings of 0.25, 0.5, and 1 wt% were all unable to prevent severe capacity degradation. While the typical near-optimum sol-gel coating thickness of 0.5 wt% showed improved initial capacity of ~190 mAh/g, this quickly faded over the course of 50 cycles at a rate comparable to cells containing bare $LiCoO_2$. As expected, unmodified $LiCoO_2$ provides a higher initial discharge capacity (~180 mAh/g instead of 140 mAh/g), but this capacity fades very rapidly at the high voltage cut-off. Al_2O_3 coated materials showed improved capacity retention comparable to previous work by our group, indicating that the LSSO coatings were indeed failing to protect the $LiCoO_2$ cathode material in some fundamental way.

3.3 Improved Performance from LSSO and Al$_2$O$_3$ Dual Coating

Before additional characterization work was utilized to better understand the differences between LSSO and Al$_2$O$_3$ coated samples, a dual-coated sample was prepared. Due to the probable lithium diffusivity of LSSO, but apparent protection of Al$_2$O$_3$ against electrolyte-driven degradation mechanisms, sequential coatings of 0.25 wt% LSSO, followed by 0.25 wt% of Al$_2$O$_3$ were applied to LiCoO$_2$. This weight percentage was chosen as our previous work has shown that roughly ~0.5 wt% seems to be an optimal loading for a ceramic cathode coating via sol-gel methods.

The dual coated material delivered an enhanced capacity with retention more in line with the expected performance of LSSO, as is also shown in **Figure 5**. The ability of an inner layer of LSSO to improve the performance of an Al$_2$O$_3$ coated material implies that some of the theoretical properties of this material may be correct, even if LSSO fails as a coating material on its own. Notably, the opposite coating orientation had improved retention but delivered less capacity, as one would expect given the difficulty of lithium diffusion through Al$_2$O$_3$. The contrast between the theoretical prediction that LSSO should be a superior coating material, and its apparent lack of an effect on its own, suggests several distinct explanations. There are three possibilities: 1) LSSO coatings fail for some reason not considered in the theoretical analysis by Aykol et. al., 2) Al$_2$O$_3$ coatings operate by a powerful mechanism not considered during the theoretical work, or 3) a coating of LSSO was not achieved on the surface of LiCoO$_2$, but rather nonconformal Li$_2$SrSiO$_4$ is present in sample. As shown in the remainder of this work, a combination of the first two possibilities appears to explain the superiority of the dual coating in this orientation.
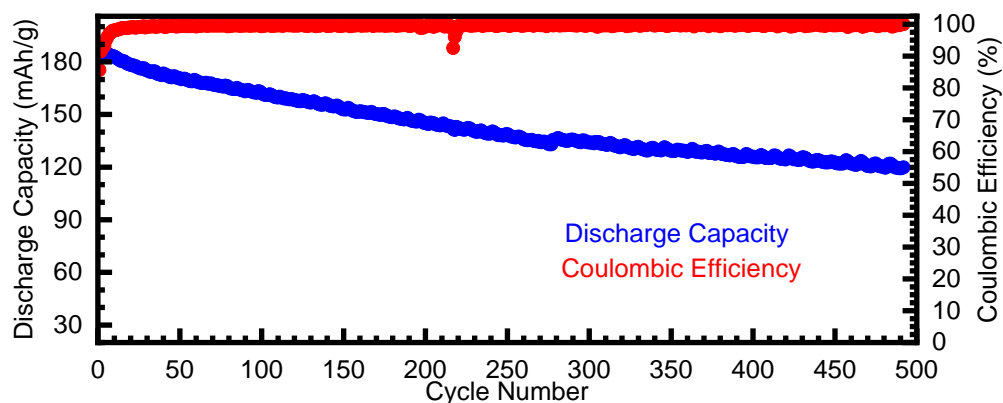

Figure 6: Long duration cycling testing of dual coated cathode material in a half cell from at 3.0-4.5V and 0.5 C.

Based on the superiority of the 0.25 wt% LSSO and 0.25 wt% Al$_2$O$_3$ coated, from here on known as the "dual coated" sample, additional electrochemical tests were performed to characterize its performance, and compare with other coating schemes. Long-duration cycling performance shown in **Figure 6** shows the excellent capacity retention of LiCoO$_2$ dual coated with LSSO and Al$_2$O$_3$ at a greater cut-off voltage. The retention is not excellent by full-cell standards because of complicating factors of half-cell testing, but the retention of the dual coating far outpaces the other coating schemes that were tested.
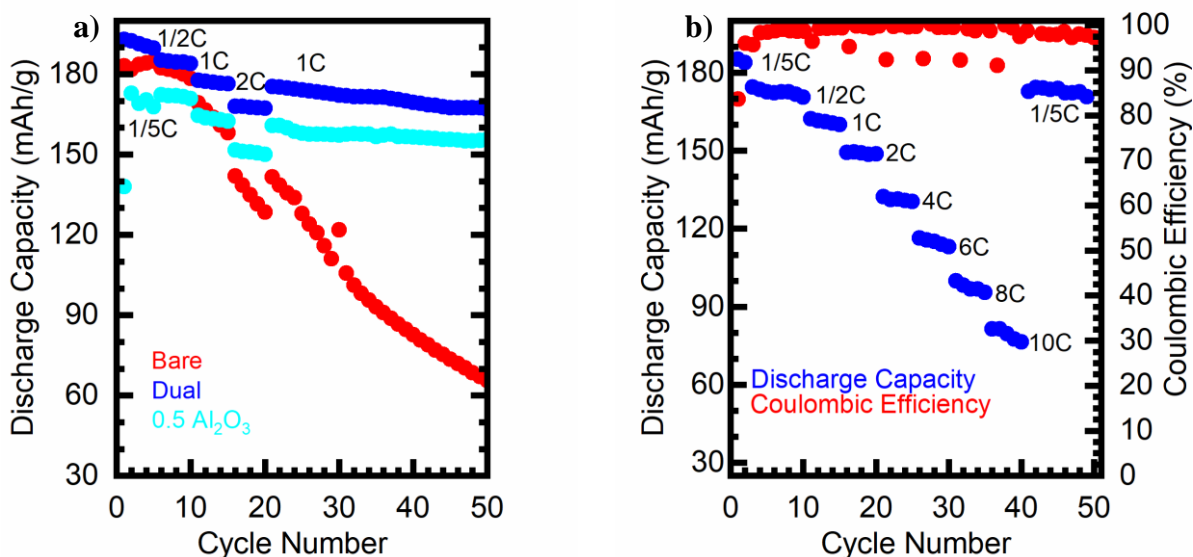
3.4 Electrochemical Characterization

Figure 7: a) Comparison between the rate capability of bare and coated materials across a voltage window of 3.0 – 4.5V. b) Excellent rate capability and high-rate capacity retention of dual coated material.

Due to the addition of potentially ion-mobility impeding ceramic layers to the cathode surface, high C-rate testing was performed to determine the extent to which these coatings limit fast charging or discharging. As shown in **Figure 7a**, both the Al$_2$O$_3$ and dual coated material showed good rate capability and minimal loss of capacity when returned from a 2C-rate to a more typical 1C. However, the dual coated material delivered a greater capacity across all rates and appears to lose less capacity with increases in charge and discharge rates. As expected, the uncoated material failed rapidly at the high voltage cut-off and the high rate of charge and discharge. Interestingly, if the rapidly declining capacity is ignored, it appears that the bare material temporarily loses more

capacity at higher rates than the coated samples. This might be indicative of the charge transfer resistance across the bare samples degraded surface phases and thicker CEI. **Figure 7b** shows the dual coated samples excellent capacity retention after very high rate cycling to a 10C-rate in steps. The ability to charge at such high rates without severe capacity degradation is superior to previous work on Al_2O_3 coatings[35].
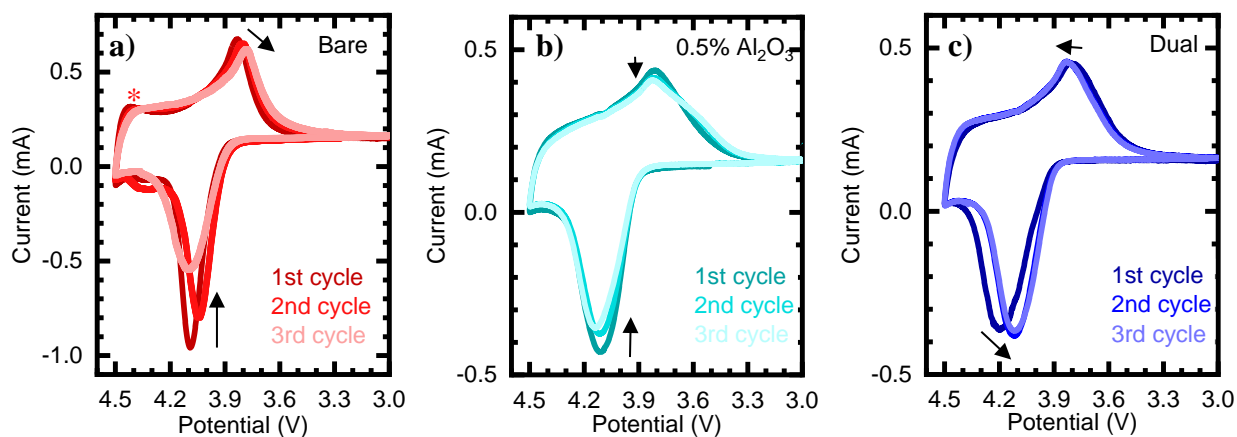

Figure 8: Cyclic voltammetry scans on a) bare, b) 0.5 wt% Al_2O_3 coated, and c) 0.25 wt% Al_2O_3 and 0.25 wt% LSSO coated materials. Results are shown for the first three cycles of half-cells from 3.0V to 4.5V at a scan rate of 0.1 mV/s which is about a ~1.5 C-rate, so kinetic limitations are present to some degree. Theses scans begin with the cell at its rest voltage of ~3V and progress counterclockwise through charge to 4.5V, and then discharge back to 3.0V.

Figure 8 shows cyclic voltammetry scans for the first three cycles on half-cells with bare, 0.5 wt% Al_2O_3 and dual coated cathodes of similar mass. Most notably in these scans, significant changes can be seen in the bare LCO sample during the first three cycles in contrast with coated samples. In **Figure 8a** the peak discharge current decreases from nearly twice that of the cells with coated cathodes to be more in line with them. This could be due to the corrosion of the uncoated cathode and the formation of a natural CEI in the bare cycle, which imposes a greater resistance to a rapid discharge. This is further implied by an anomalous peak at ~4.4V which is likely caused by oxidation of electrolyte at the surface of the cathode. In **Figure 8b** the cell with the 0.5 wt% Al_2O_3 coated cathode appears to undergo less dramatic changes during the first three cycles. The peak current on discharge decreases, although much less dramatically, possibly indicating the formation of a less thick CEI on the surface of the Al_2O_3. The peak current on charge appears blunted, likely due by the resistance to lithium diffusion through the coating, which seems to increase slightly over time. The scan of the cell with dual coated material shown in **Figure 8c** is similar to that of

the Al$_2$O$_3$ coated sample, with a couple of slight differences. First, both the peak charge and discharge current increase from the first to the second cycle. This suggests that the resistance to lithium diffusion into the cathode material may have decreased after the first cycle. Additionally, very little change is seen from the second to the third cycle, as is expected from the superior cycling stability of this material.
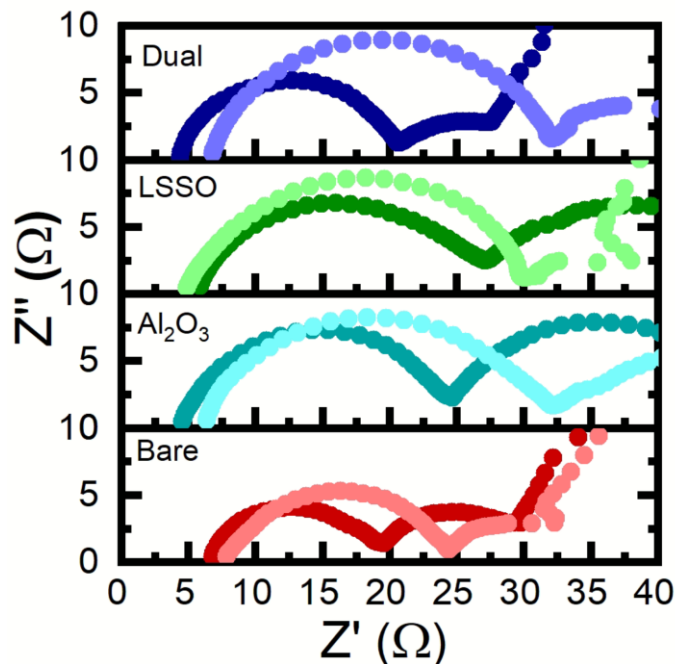

Figure 9: Electrochemical impedance spectroscopy on 3 investigated 0.5 wt% coatings and bare LiCoO$_2$ in half cells. Dark and light markers indicate coin cells that were test as fabricated and after 50 cycles at 3.0-4.5V and 0.5C respectively.

To better understand the impedance present in cells made from cathode material of each coating type EIS was performed before and after 50 cycles at a 4.5V cut-off. While fitting was not performed on the spectra due to the complex shapes and noise in the data, the size of the features is indicative of the magnitude of present impedance sources. The most important feature of these spectra, the two semi circles in each, are generally indicative of lithium-ion transport through the CEI/coating film (left) and the cathode-coating/CEI interface. As expected, the impedance of all the cells grew over the course of the 50 cycles, as the CEI grew, and cathode surface degradation progressed. The bare sample had the lowest impedance initially across both boundaries, and the least growth in each. This is unsurprising given that it does not have a ceramic coating, and the effects of degraded phases in the LCO itself would only be visible at lower frequencies off to the right. However, this does indicate that the interfacial resistance resulting from the CEI in bare LCO

does not appear to be a main cause for reduced discharge capacity. The Al_2O_3 and LSSO coated samples had comparable impedance across both boundaries initially. However, the coating-cathode interfacial resistance continues to grow in the Al_2O_3 coated sample, while it shrinks and takes on a new and strange shape in the LSSO coated sample. The growing $Al_2O_3 - LCO$ interfacial resistance might be explained by reactions/mixing during cycling, as will be described later. However, the complex shape of the impedance feature in the LSSO coated sample may be due to the lack of a thick, impeding interface. The lower initial impedance across both boundaries observed in the dual coated sample is interesting, as it may be the result of low impedance to lithium transport through both the coating layers and the interface with the cathode surface itself. The growth in the impedance of the CEI/electrode feature after cycling is similar to the other coating schemes, however the impedance of the cathode-coating interface feature is more similar to LSSO. This lends some support for the theory that the outer Al_2O_3 coating serves the role of forming a beneficial (while slightly lithium-ion impeding) CEI, while the inner LSSO separates the Al_2O_3 from the surface of the cathode so that complex and impeding mixed interfaces do not form.

3.5 Particle Imaging

To gain further insight into the morphology and function of the coatings on these materials, X-ray fluorescence and ptychography were performed using synchrotron radiation from the Advanced Photon Source at Argonne National Laboratory. X-ray fluorescence measurements allowed for the mapping of elements to determine the distribution and composition of the applied coatings. X-ray ptychography allowed for direct imaging of the coating layer on pristine and cycled samples.
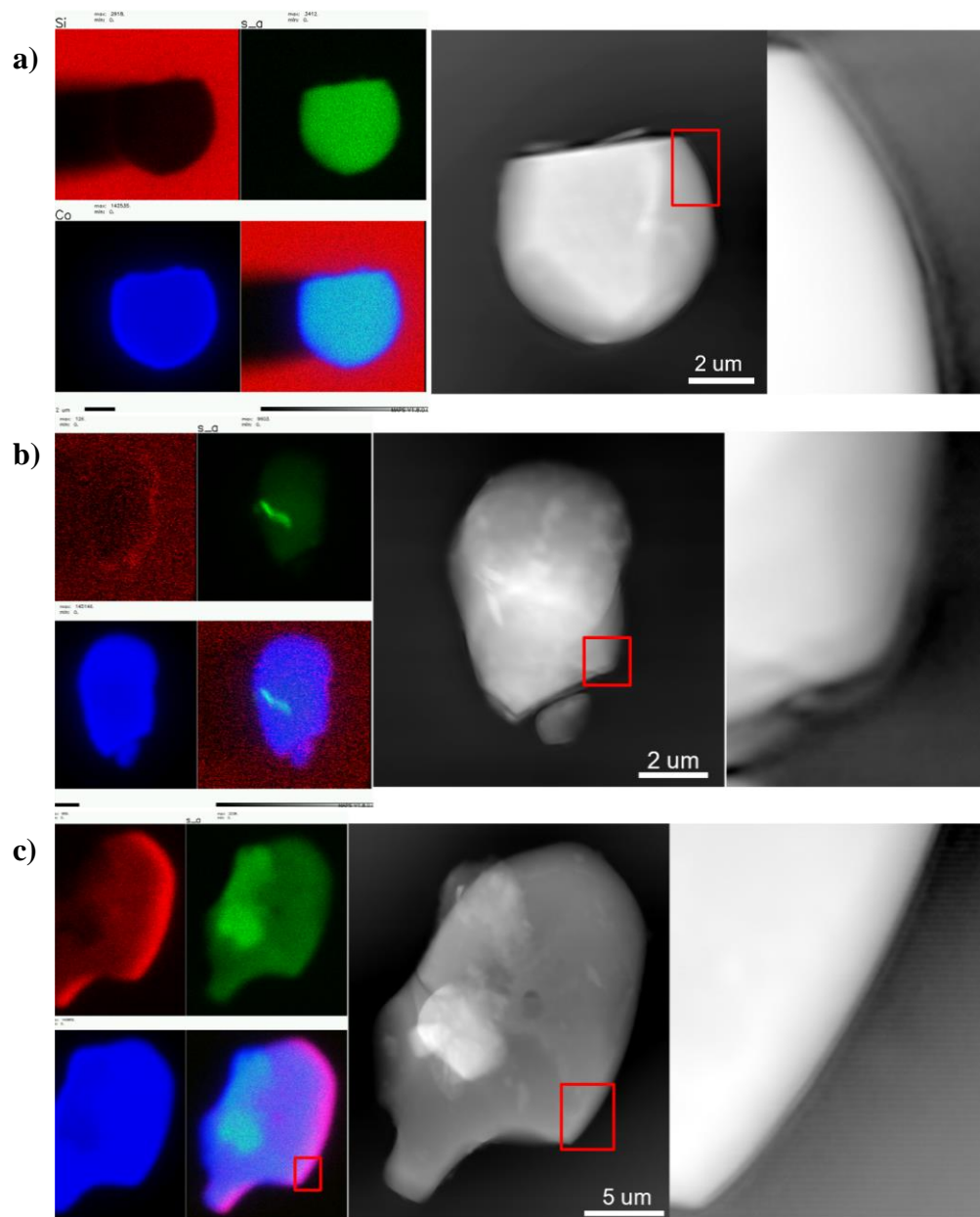
Figure 10: X-ray fluorescence mapping (color) and ptychography (gray) on pristine a) LSSO coated, b) Al_2O_3 coated, and c) dual coated cathode particles. The cathode coating can be seen in the samples as indicated.

The images displayed in **Figure 10** show individual as-coated cathode samples with elemental mapping and a visible coating layer. In **Figure 10a**, the LSSO coated sample, red corresponds to silicon, green to oxygen, and blue to cobalt. Due to the use of a silicate sample holder, the silicon in the surface layer is unfortunately not visible in the elemental mapping. Cobalt and oxygen are evenly distributed as expected. The coating can be clearly seen as a thin layer (measured to be

~100 nm in most locations) on the outside of the particle. In **Figure 10b**, the Al_2O_3 coated sample, red represents aluminum, green oxygen, and blue cobalt. The Al_2O_3 coating layer is barely visible elemental mapping, although it can be made out around the edge of the particle. The coating layer seen in the ptychography image is roughly the same thickness as the layer observed in the LSSO coated sample, as expected. In **Figure 10c**, the dual coated sample, the colors represented are the same as for the Al_2O_3 coated sample. The elemental mapping cannot resolve any clear coating layer of the aluminum in this sample either, although it appears to be concentrated towards the edge of the particle. The ptychography images of this material also appear to show two coating layers on the surface of the particle. However, it is not possible to definitively tell if these are LSSO and Al_2O_3.
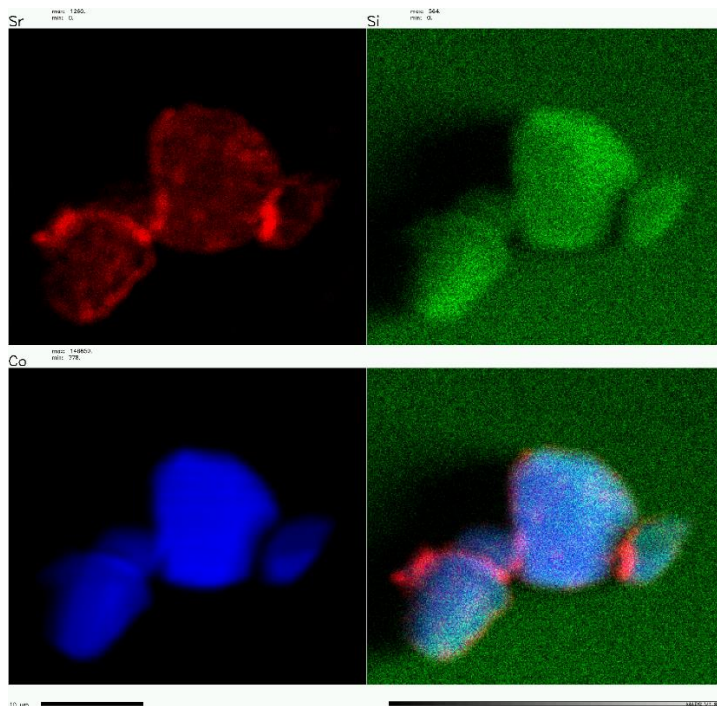

Figure 11: X-ray fluorescence mapping on pristine dual coated cathode particles. Inhomogeneities in the distribution of strontium (red) can be observed. Green shows silicon and blue shows cobalt. Lower right depicts the combination of the three measured elements.

Due to the inability to see silicon in the sample because of the background, more fluorescence images were measured for the dual coated sample including the characteristic energy of strontium. While the strontium appears to be distributed broadly over the surface of the particle, it is concentrated in certain areas. The silicon in this image (green) is easier to see and appears

homogeneous, but this could be due to the background noise from the sample holder. This suggests that the LSSO coating layer, and possibly also the Al_2O_3 layer, are significantly inhomogeneous. This agrees with observations from the ptychography images, with some locations on the particles appear to have coatings of >100 nm, while in other places the coating cannot be seen (although it may be present but very thin).
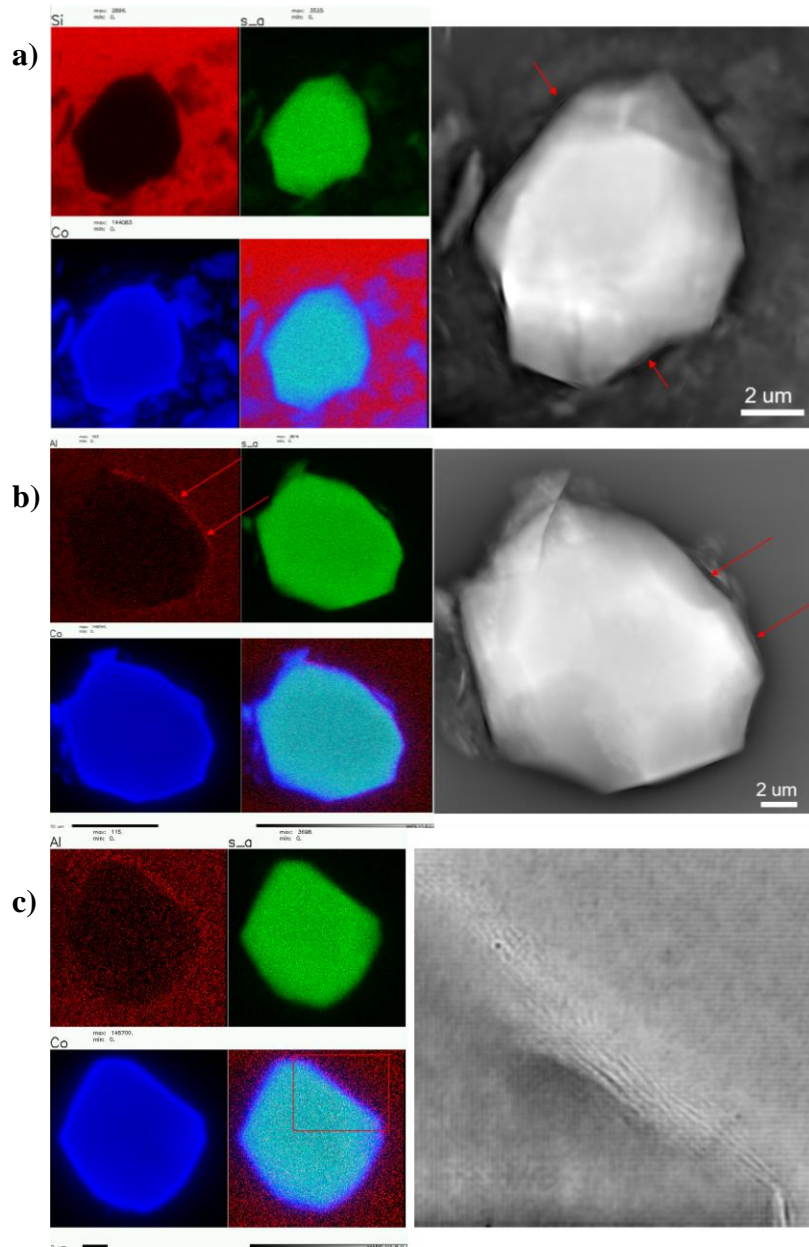

Figure 12: X-ray fluorescence mapping (color) and ptychography (gray) on 50th cycle a) LSSO coated, b) Al2O3 coated, and c) dual coated cathode particles. The cathode coating can be seen in the samples as indicated.

Using the same measurement techniques as in **Figure 10**, cycled cathode material was imaged to see if any changes could be observed. While the elemental mapping looked quite similar to the pristine samples, it was clearer in these images that an aluminum containing layer was present on the surface of the Al_2O_3 coated particles. The coating layers are still visible in the images from ptychography, but they are "fuzzier" after 50 cycles, especially for the dual coated sample. This could be due to corrosion by electrolyte species, or in the case of dual coated material, a new interface forming between the two coatings.

3.6 X-Ray Absorbance Spectroscopy

To further elucidate the mechanism by which these coatings protect the cathode, at both the interface with the electrolyte and with the cathode, several XAS techniques were utilized on pristine LCO and cycles samples of the various coating schemes.
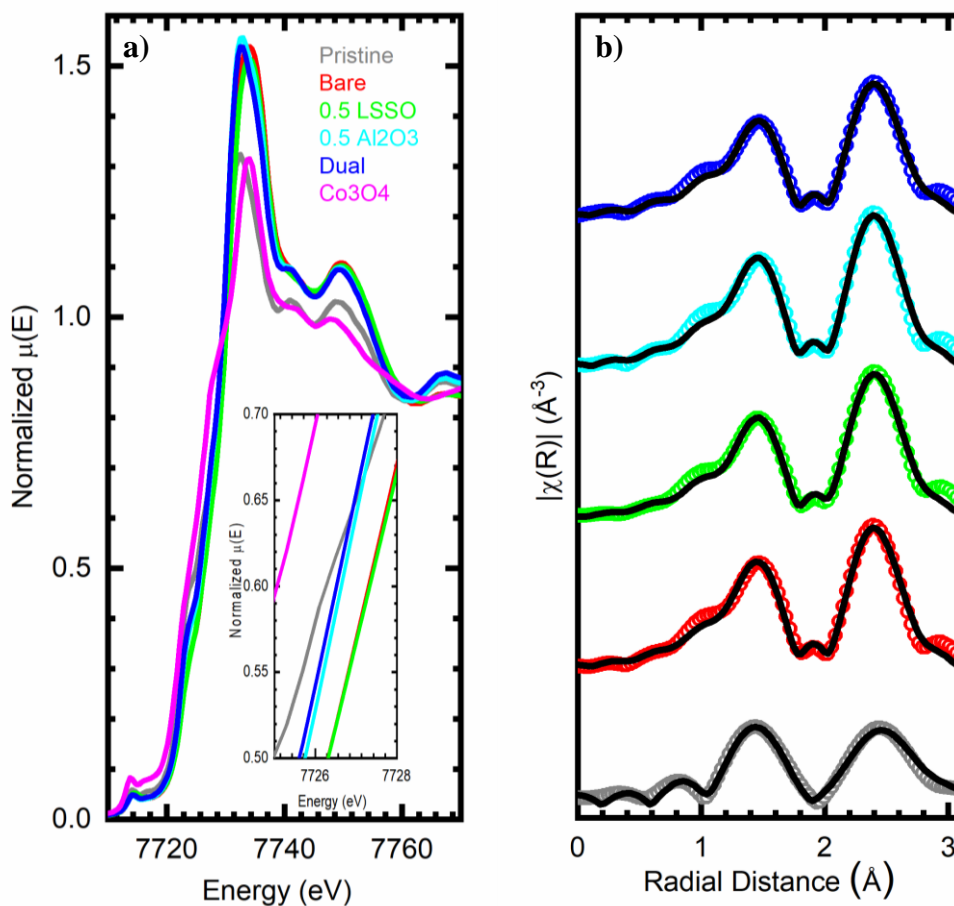

Figure 13: a) Cobalt K-edge h-XAS of pristine LCO and cycled coated materials in a discharged state after 50 cycles, along with a Co_3O_4 standard. b) fitting of EXAFS region using Athena.

As shown in **Figure 13a**, hard XAS performed in fluorescence mode on the cobalt K-edge of pristine LCO and cycled materials shows a peak shift for materials of certain coating schemes but not others. The worse performing materials electrochemically, LSSO coated and bare, show a shift towards the undesired 2^+ oxidation state represented here by the Co_3O_4 standard. The Al_2O_3 and dual coated material show no such peak shift, suggesting they retain the cobalt environment of the pristine material. These are the coatings with exterior Al_2O_3, so this material does seem to play an important role in preventing cobalt reduction by the electrolyte. LSSO alone appears unable to prevent significant cobalt reduction during cycling, consistent with its poor capacity retention. The bulk sensitivity of this measurement means that it is more summative of the overall change in the cobalt environment, so the alignment with cycling performance is expected. Fitting performed on the EXAFS region, **Figure 13b**, showed minor changes but largely similar spectra compared to pristine, suggesting no significant bulk structure changes in LCO.

To better understand the change in the environment closer to the surface, rather than in the bulk as the hard XAS cobalt K-edge shows, soft XAS was performed on the Cobalt $L_{3,2}$-edge and Oxygen K-edge in electron yield mode.
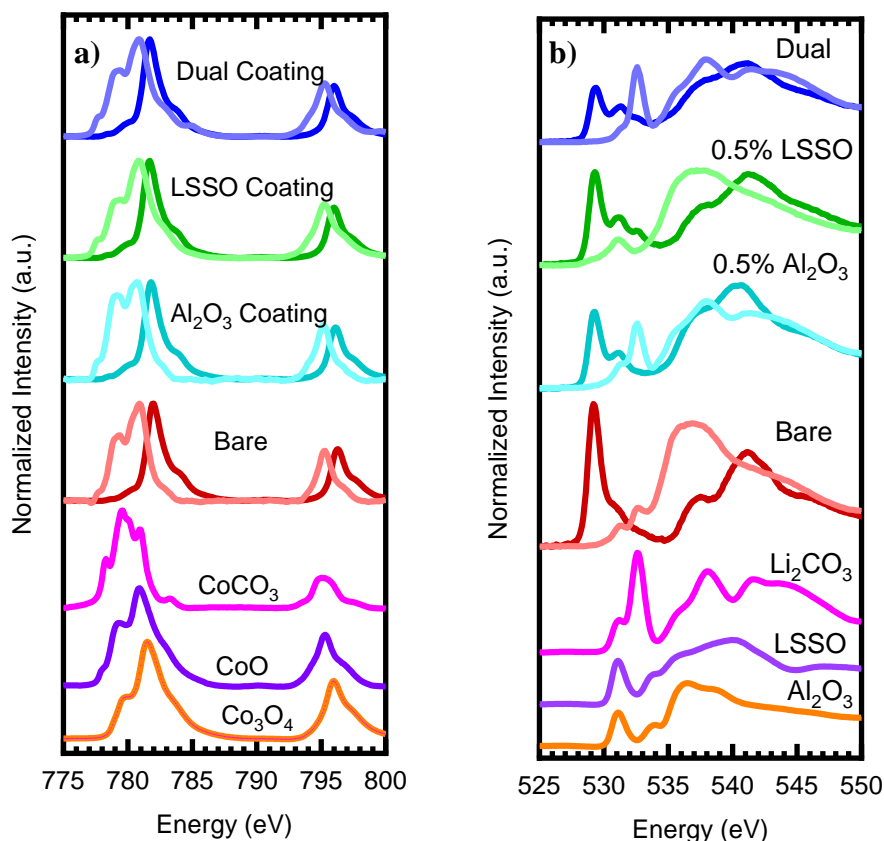
Figure 14: Electron Yield Soft XAS on bare and coated samples before (dark) and after (light) cycling with relevant references at the a) Cobalt $L_{3,2}$-edge and b) Oxygen K-edge.

The cobalt $L_{3,2}$-edge spectra of pristine and 50th cycle samples shown in **Figure 14a** shows that the edge of all coated samples initially matches the uncoated material. This suggests that Co-O hybridization, and therefore the structure and stoichiometry of near-surface $LiCoO_2$, remains relatively unchanged during the coating process itself. However, after cycling, all the samples shifted to lower energies and developed a satellite peak to differing extents. The shift appears the most pronounced in the bare and Al_2O_3 coated material, and less in the dual and LSSO coated. The shift and the new peak do not perfectly line up with any of the references but appear similar in energy to the $CoCO_3$ and CoO references, which have an oxidation state of 2^+. This is surprising because it indicates that even in the dual coated sample there is widespread degradation of near surface $LiCoO_2$ to electrochemically inactive phases after 50 cycles. Because this change of oxidation state occurs during cycling, not during heating to 600°C, it is unlikely to be mainly because of a reaction between the coating and $LiCoO_2$ phases. Instead, it could be due to corrosion by electrolyte

decomposition products or loss of lattice oxygen due to stacking rearrangements that is not prevented by the coating during cycling.

The oxygen K-edge spectra of pristine and cycled samples in **Figure 14.b.** shows that like the cobalt $L_{3,2}$-edge, a common peak exists across all pristine samples corresponding to Co-O bonding. Depending on the composition of the coating layers, the pristine spectra also contain peaks indicative of Al-O or Si-O bonds at ~531 eV. Additionally, the strength of the Co-O peak fades due to attenuation through coatings in these samples, as would be expected. The broad feature to the right could not be identified with certainty, and likely results from a mix of different oxygen environments. After cycling, the Co-O peak disappears in all samples. In the cycled bare sample, it is replaced with a small peak corresponding to Li_2CO_3 and another broad feature at around 535-540 eV. This combination is indicative of the formation of the complex lithium/organic CEI known to form on the surface of LCO. In the Al_2O_3 coated sample, the Al-O peak is barely retained and the Li_2CO_3 peak is much larger. This seems to indicate that the coating dramatically changes the formation and composition of the CEI. In the LSSO coated sample, there is no discernable Li_2CO_3 peak, the Si-O peak is retained, and a broad feature more like the bare material formed. Combined, these changes seem to suggest that the CEI formed on LSSO coated material alone is somehow different and unbeneficial, as will be discussed later. In the dual coated sample, the Li_2CO_3 peak is even stronger, and the broad feature has a shape similar to that of the cycled Al_2O_3 coated material. Taken together, these spectra implicate that the dual coating produces a coating-electrolyte interface that is similar to that of Al_2O_3 coated material.
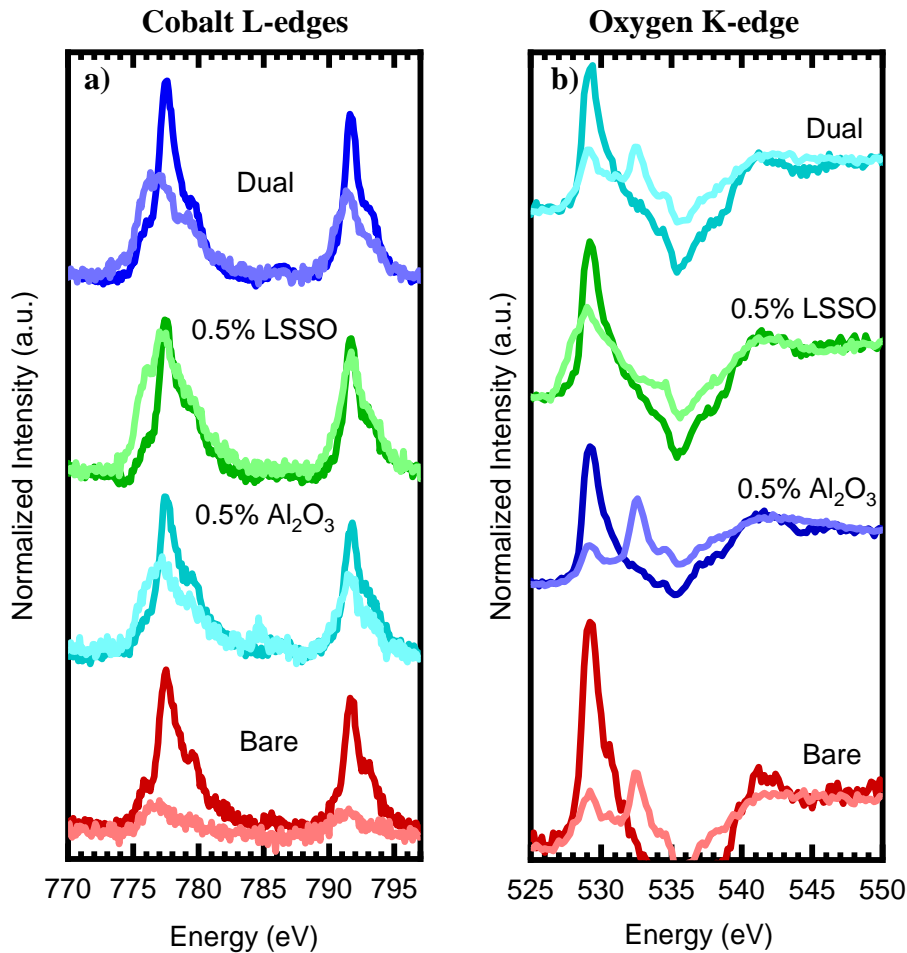
Figure 15: Fluorescence yield soft XAS on bare and coated LCO before (dark) and after (light) 50 cycles at the a) cobalt $L_{3,2}$-edges and b) oxygen K-edge.

Due to the surface sensitivity of the electron yield soft XAS from **Figure 14**, fluorescence yield data was also measured to ensure changes to the environment of cobalt and oxygen deeper in the material were not missed. In the cobalt $L_{3,2}$-edges from fluorescence in **Figure 15**, the energy of the peaks appear only slightly shifted, indicative of less reduction of bulk cobalt. However, the signals are weakened to very different extents that could indicate different attenuation lengths resulting from differing CEI thicknesses. The LSSO coated sample appears almost unaffected, while the bare sample is almost lost to background noise. Despite their similar cycling behavior, this suggests that LSSO forms a very thin CEI, while bare material has a very thick one after 50 cycles. The oxygen K-edge data with

this more bulk sensitive method corroborates previous conclusions about the differing CEI compositions and thicknesses of the different coating schemes.

3.7 The Role of Strontium in LSSO

The original theoretical basis for the selection of LSSO as a coating involved its lithium content and the HF scavenging ability of its Si-O bonds. While the strontium content may play some role in the predicted stability of the coating on the surface of cathode materials, it seemed to not be critical to the functions of the dual coating identified so far in this work. As such, Li_4SiO_4 (LSO) was applied as a coating via the same method as LSSO but with more lithium salts in place of strontium, both on its own and as a dual coating.
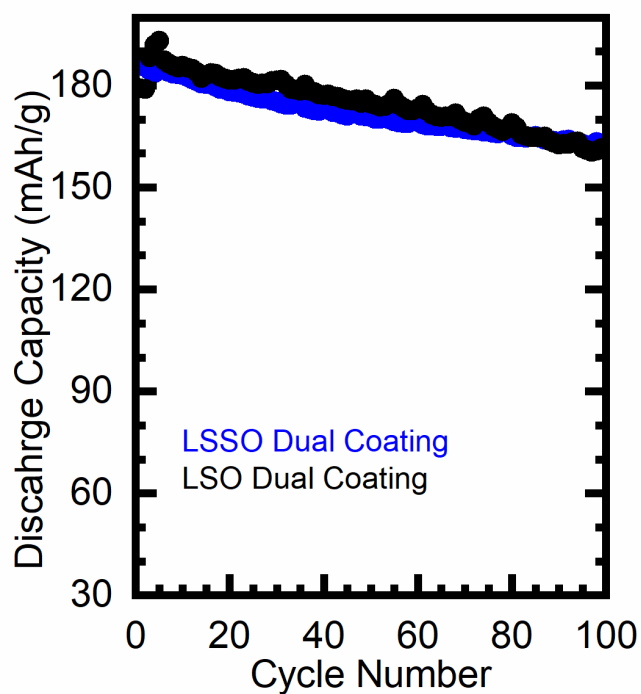
Figure 16: Long duration cycling comparison of dual coatings of Li_2SrSiO_4 / Li_4SiO_4 and Al_2O_3 at 3.0-4.5V at 0.5 C rate.

A comparison between the long duration cycling performance of LSO and LSSO in a dual coating with Al_2O_3 is shown in **Figure 16**. While material coated with 0.5 wt% LSO failed just as LSSO does, the dual coatings perform almost identically over 100 cycles at high cut-off voltage. This supports the idea that only the lithium content and Si-O bonds of the LSSO are contributing to the superior performance of dual coated material, and strontium plays little to no role.

3.8 The Mechanism of Dual Coatings

Based on the performance and characterizations on these coating schemes, a general mechanism for protection of the cathode by the dual coating can be put forward. Based on the evidence obtained from these measurements, the proposed mechanism appears to be quite complex and occurs by several different potential routes.

First, the superior initial discharge capacity of LSSO coated samples, the lower first cycle impedance of dual coated samples, and the natural lithium content of LSSO all suggest that its lithium-ion conductivity may be superior to Al_2O_3. Based on this, one would expect LSO, with more available lithium to aid in ion diffusion and a similar crystal structure, to be a superior coating for capacity retention to LSSO. It may be that further testing would show that it is. However, given the extremely high-rate capability of dual coated material, diffusion across LSSO and LSO is likely not a limiting factor in the performance of the dual coating. However, the LSSO may also be aiding in the necessary lithium doping of Al_2O_3. If this is indeed important, then the $Li_xAl_yO_z$ composition space should be explored further as cathode coatings.

Second, there seems to be some benefit to the separation of Al_2O_3 (at least when applied via a sol-gel method) from the surface of the cathode material. The similar performance of the dual coating in the opposite orientation, with LSSO on the outside, to Al_2O_3 coated material suggests that LSSO plays an important role beneath the Al_2O_3 layer. If it is assumed, as the X-ray fluorescence images suggest, that the LSSO covers most of the surface of the dual coated particles, then the Al_2O_3 does not contact the surface of the LCO in dual coated samples. Because the free energy of reaction suggests that Al_2O_3 will react with LCO itself to for intermediate phases[35], the LSSO coating is likely preventing such reactions from occurring during the heating process or battery cycling. The same logic suggests that LSSO would not react at the boundary with LCO to the same extent, as all possible reaction products are higher in energy. If this aspect of the dual coating is significant in its performance, then it is also reasonable to ask whether LSSO and Al_2O_3 might be reacting to form products at the interface or even in their entirety. Reactions involving most of both coatings are unlikely, as the performance of a dual coating of the opposite coating orientation should then be similar. However, reactions at the boundary cannot be ruled out entirely by the resolution of the available methods, especially considering that the energy of possible reaction products ($SrSiO_3$

and LiAlO$_2$) is lowered. Regardless, there appears to be a benefit to avoiding contact between the cathode surface and Al$_2$O$_3$ (at least using a practical sol-gel method with the necessary heating). Therefore, the thinking of Aykol et. al. to exclude coating materials which can react with LCO is merited.

Additionally, it seems that the CEI formed by materials coated with LSSO is thinner, different in composition, and unable to protect the cathode from continuous surface degradation. The observed properties of the CEI using XAS show that the CEI of dual coated and Al$_2$O$_3$ coated materials is thicker, contains significant Li$_2$CO$_3$, and prevents rampant reduction of cobalt. This suggests that the CEI formed by Al$_2$O$_3$ (and possibly other simple oxides that are effective coating materials i.e. ZrO$_2$, TiO$_2$) is unique in its ability to slow the decomposition of electrolyte species and surface corrosion of the cathode. While the measurements performed in this work are unable to probe exactly how this occurs, this is useful information in the search for better coating materials. It may be that the LSSO is too effective in its HF scavenging ability, or accelerates the decomposition of the electrolyte, and therefore is sacrificed at the expense of protecting the cathode. The extent to which the Si-O bonds, the predicted HF scavenging site of LSSO, contribute to this phenomenon is unknown. However, if HF scavenging by LSSO is widespread in such materials, it is worth noting that the lithium content of the coating and lithium diffusion will be reduced. This is according to charge balance in Li$_{2-x}$SrSiO$_{4-x}$F$_x$, and in agreement with EIS data which shows LSSO coated material has the greatest ionic impedance after 50 cycles. Despite uncertainty in the exact route, it seems that LSSO and LSO fail to prevent the degradation pathways of layered cathodes charged to high cut-off voltages.

Given the inhomogeneities observed in the imaging techniques performed on the LSSO and dual coated samples, it is worth questioning whether dual coating a material simply allows for better total coverage. While a sequential coating of the same material twice was not performed in this work, it is unlikely that this effect is significant. If patching was the main reason the dual coating works better than Al$_2$O$_3$ coatings alone, then one would expect dual coated materials in the opposite orientation to have comparable performance, and they do not. Additionally, one would expect LSSO coatings to at least help somewhat if this were the main reason for the success of the dual

coating, yet they seem to have very little effect. Therefore, the dual coating appears to have unique functionalities stemming from each of the layers.

Conclusion

The theoretical prediction that LSSO should be a superior coating to the existing Al_2O_3, on account of its HF scavenging, lithium conductivity, and lack of reaction with LCO has been shown to be flawed. While these three properties do seem consistent with the observed properties of LSSO coated LCO, its interaction with the electrolyte and CEI formation make it an ineffective coating. Based on the focus on LCO-compatibility of the theoretical work this project was based on, LSSO was applied as the first layer in a dual coating with Al_2O_3 on the outside, serving as the primary contact with the electrolyte. This dual coated material proved to have superior cycling performance to Al_2O_3 coated material, exceptional rate capability, and formed a CEI very similar to Al_2O_3 coated material. The beneficial nature of Al_2O_3 cathode coatings with the electrolyte is therefore more important than was assumed. It may be that some aspect of the interaction of orthosilicates with the electrolyte at high voltage causes their own rapid degradation and abrupt failure to protect the surface of the cathode. These findings underscore the difficulty of identifying an appropriate cathode coating material that can fulfill all the requirements for stable cycling at high voltages. Based on these findings, lithium containing simple oxides (i.e. $Li_xAl_yO_z$) or lithium-aluminosilicates (i.e. $Li_xAl_ySi_zO_4$) are implicated as potential cathode coating compositions for future research

As the rarity of nickel begins to constrain the lithium-ion battery industry in terms of total possible production, but also in cost, the industry will be forced to seek out new cathode chemistries without both nickel and cobalt as the redox reservoir. As this is occurring, new applications demanding greater energy density will continue to drive innovation in long lasting, energy dense intercalation chemistries. Without the convenient layered structure that only nickel, and cobalt allow, the attainable capacity of novel cathode chemistries will likely be limited, have more sharply slanted voltage profiles, and require smaller particle sizes. Together, these drivers will require stabilizing a greater cathodic surface area, at higher voltages, and with potentially less stable crystal structures. Therefore, research on surface modifications to high voltage cathode species will

remain important for the commercialization of new cathodes chemistries that simultaneously have greater energy density, no rare metals, and long useful lifespans.

References

1. Rogelj, J.; den Elzen, M.; Höhne, N.; Fransen, T.; Fekete, H.; Winkler, H.; Schaeffer, R.; Sha, F.; Riahi, K.; Meinshausen, M. Paris Agreement Climate Proposals Need a Boost to Keep Warming Well below 2 °C. Nature 2016, 534 (7609), 631–639.

2. Chu, S.; Cui, Y.; Liu, N. The Path towards Sustainable Energy. Nature Materials 2016, 16 (1), 16–22.

3. Eberhard, M.; Tarpenning, M. The 21st Century Electric Car Tesla Motors . (accessed May 10, 2021).

4. Whittingham, S. M. Intercalation Chemistry and Energy Storage. *Journal of Solid State Chemistry* **1979**, *29* (3), 303–310.

5. Mizushima, K.; Jones, P.; Wiseman, P.; Goodenough, J. Li_xCoO_2 ($0{<}x{\leqslant}1$): A new cathode material for batteries of high energy density (Solid State Ionics **1981**, *3-4*, 171–174.

6. Yoshino, A. The Birth of the Lithium-Ion Battery. *Angewandte Chemie International Edition* **2012**, *51* (24), 5798–5800.

7. Ziegler, M. S.; Trancik, J. E. Re-Examining Rates of Lithium-Ion Battery Technology Improvement and Cost Decline. Energy & Environmental Science 2021, 14 (4), 1635–1651.

8. Pillot, C. The Rechargeable Battery Market and Main Trends 2018-2030. 36th Annual International Battery Seminar, 2019

9. Cole, W.; Frazier, A. Cost Projections for Utility-Scale Battery Storage: 2020 Update. *National Renewable Energy Laboratory* **2020**.

10. Manthiram, A., A reflection on lithium-ion battery cathode chemistry. *Nat Commun* **2020,** *11* (1), 1550.

11. Li, W.; Erickson, E. M.; Manthiram, A. High-Nickel Layered Oxide Cathodes for Lithium-Based Automotive Batteries. *Nature Energy* **2020**, *5* (1), 26–34.

12. Lim, J.-M.; Hwang, T.; Kim, D.; Park, M.-S.; Cho, K.; Cho, M. Intrinsic Origins of Crack Generation in Ni-Rich LiNi0.8Co0.1Mn0.1O2 Layered Oxide Cathode Material. *Scientific Reports* **2017**, *7* (1).

13. Naumann, M.; Spingler, F. B.; Jossen, A. Analysis and Modeling of Cycle Aging of a Commercial LiFePO4/Graphite Cell. *Journal of Power Sources* **2020**, *451*.

14. Lu, Z.; MacNeil, D. D.; Dahn, J. R. Layered $LiNi_xCo_{1-2x}Mn_xO_2$ Cathode Materials for Lithium-Ion Batteries. *Electrochemical and Solid-State Letters* **2001**, *4* (12).

15. Banza Lubaba Nkulu, C.; Casas, L.; Haufroid, V.; De Putter, T.; Saenen, N. D.; Kayembe-Kitenge, T.; Musa Obadia, P.; Kyanika Wa Mukoma, D.; Lunda Ilunga, J.-M.; Nawrot, T. S.; Luboya Numbi, O.; Smolders, E.; Nemery, B. Sustainability of Artisanal Mining of Cobalt in DR Congo. *Nature Sustainability* **2018**, *1* (9), 495–504.

16. Li, H.; Liu, A.; Zhang, N.; Wang, Y.; Yin, S.; Wu, H.; Dahn, J. R. An Unavoidable Challenge for Ni-Rich Positive Electrode Materials for Lithium-Ion Batteries. Chemistry of Materials 2019, 31 (18), 7574–7583.

17. Patry, G.; Romagny, A.; Martinet, S.; Froelich, D. Cost Modeling of Lithium-Ion Battery Cells for Automotive Applications. Energy Science & Engineering 2014, 3 (1), 71–82.

18. Li, S.; Luo, Z.; Li, L.; Hu, J.; Zou, G.; Hou, H.; Ji, X. Recent Progress on Electrolyte Additives for Stable Lithium Metal Anode. *Energy Storage Materials* **2020**, *32*, 306–319.

19. Xu, C.; Reeves, P. J.; Jacquet, Q.; Grey, C. P. Phase Behavior during Electrochemical Cycling of Ni-Rich Cathode Materials for Li-Ion Batteries. *Advanced Energy Materials* **2020**, *11* (7).

20. Zhitao, E.; Guo, H.; Yan, G.; Wang, J.; Feng, R.; Wang, Z.; Li, X. Evolution of the Morphology, Structural and Thermal Stability of LiCoO2 during Overcharge. *Journal of Energy Chemistry* **2020**, *55*, 524–532.

21. Heenan, T. M.; Wade, A.; Tan, C.; Parker, J. E.; Matras, D.; Leach, A. S.; Robinson, J. B.; Llewellyn, A.; Dimitrijevic, A.; Jervis, R.; Quinn, P. D.; Brett, D. J.; Shearing, P. R. Identifying the Origins of Microstructural Defects Such as Cracking within Ni-Rich NMC811 Cathode Particles for Lithium-Ion Batteries. *Advanced Energy Materials* **2020**, *10* (47).

22. Xu, C.; Märker, K.; Lee, J.; Mahadevegowda, A.; Reeves, P. J.; Day, S. J.; Groh, M. F.; Emge, S. P.; Ducati, C.; Layla Mehdi, B.; Tang, C. C.; Grey, C. P. Bulk Fatigue Induced by Surface Reconstruction in Layered Ni-Rich Cathodes for Li-Ion Batteries. Nature Materials 2020, 20 (1), 84–92.

23. Xiao, P.; Shi, T.; Huang, W.; Ceder, G. Understanding Surface Densified Phases in Ni-Rich Layered Compounds. ACS Energy Letters 2019, 4 (4), 811–818.

24. Liu, M.; Vatamanu, J.; Chen, X.; Xing, L.; Xu, K.; Li, W. Hydrolysis of LiPF6-Containing Electrolyte at High Voltage. ACS Energy Letters 2021, 2096–2102.

25. Amatucci, G. Cobalt Dissolution in LiCoO2-Based Non-Aqueous Rechargeable Batteries. *Solid State Ionics* **1996**, *83* (1-2), 167–173.

26. Faenza, N. V.; Bruce, L.; Lebens-Higgins, Z. W.; Plitz, I.; Pereira, N.; Piper, L. F.; Amatucci, G. G. Growth of Ambient Induced Surface Impurity Species on Layered Positive Electrode Materials and Impact on Electrochemical Performance. *Journal of The Electrochemical Society* **2017**, *164* (14).

27. An, S. J.; Li, J.; Daniel, C.; Mohanty, D.; Nagpure, S.; Wood, D. L. The State of Understanding of the Lithium-Ion-Battery Graphite Solid Electrolyte Interphase (SEI) and Its Relationship to Formation Cycling. *Carbon* **2016**, *105*, 52–76.

28. Wise, A. M.; Ban, C.; Weker, J. N.; Misra, S.; Cavanagh, A. S.; Wu, Z.; Li, Z.; Whittingham, M. S.; Xu, K.; George, S. M.; Toney, M. F. Effect of Al2O3 Coating on Stabilizing LiNi0.4Mn0.4Co0.2O2 Cathodes. *Chemistry of Materials* **2015**, *27* (17), 6146–6154.

29, Gao, H.; Zeng, X.; Hu, Y.; Tileli, V.; Li, L.; Ren, Y.; Meng, X.; Maglia, F.; Lamp, P.; Kim, S.-J.; Amine, K.; Chen, Z. Modifying the Surface of a High-Voltage Lithium-Ion Cathode. *ACS Applied Energy Materials* **2018**, *1* (5), 2254–2260.

30. Schipper, F.; Bouzaglo, H.; Dixit, M.; Erickson, E. M.; Weigel, T.; Talianker, M.; Grinblat, J.; Burstein, L.; Schmidt, M.; Lampert, J.; Erk, C.; Markovsky, B.; Major, D. T.; Aurbach,

D. From Surface ZrO2 Coating to Bulk Zr Doping by High Temperature Annealing of Nickel-Rich Lithiated Oxides and Their Enhanced Electrochemical Performance in Lithium Ion Batteries. *Advanced Energy Materials* **2017**, *8* (4).

31. Yano, A.; Shikano, M.; Ueda, A.; Sakaebe, H.; Ogumi, Z. LiCoO2 Degradation Behavior in the High-Voltage Phase Transition Region and Improved Reversibility with Surface Coating. *Journal of The Electrochemical Society* **2016**, *164* (1).

32. Jung, Y. S.; Lu, P.; Cavanagh, A. S.; Ban, C.; Kim, G.-H.; Lee, S.-H.; George, S. M.; Harris, S. J.; Dillon, A. C. Unexpected Improved Performance of ALD Coated LiCoO2/Graphite Li-Ion Batteries. *Advanced Energy Materials* **2012**, *3* (2), 213–219.

33. Johnson, R. W.; Hultqvist, A.; Bent, S. F. A Brief Review of Atomic Layer Deposition: from Fundamentals to Applications. *Materials Today* **2014**, *17* (5), 236–246.

34. Jian, Z.; Wang, W.; Wang, M.; Wang, Y.; AuYeung, N.; Liu, M.; Feng, Z. Al2O3 Coated LiCoO2 as Cathode for High-Capacity and Long-Cycling Li-Ion Batteries. *Chinese Chemical Letters* **2018**, *29* (12), 1768–1772.

35. Aykol, M.; Kim, S.; Hegde, V. I.; Snydacker, D.; Lu, Z.; Hao, S.; Kirklin, S.; Morgan, D.; Wolverton, C. High-Throughput Computational Design of Cathode Coatings for Li-Ion Batteries. *Nature Communications* **2016**, *7* (1).

36. Xu, S.; Jacobs, R. M.; Nguyen, H. M.; Hao, S.; Mahanthappa, M.; Wolverton, C.; Morgan, D. Lithium Transport through Lithium-Ion Battery Cathode Coatings. *Journal of Materials Chemistry A* **2015**, *3* (33), 17248–17272.

37. Momma, K.; Izumi, F. VESTA 3for Three-Dimensional Visualization of Crystal, Volumetric and Morphology Data. *Journal of Applied Crystallography* **2011**, *44* (6), 1272–1276.

38. Wang, M.; Árnadóttir, L.; Xu, Z. J.; Feng, Z. In Situ X-Ray Absorption Spectroscopy Studies of Nanoscale Electrocatalysts. *Nano-Micro Letters* **2019**, *11* (1).

39. Radin, M. D.; Hy, S.; Sina, M.; Fang, C.; Liu, H.; Vinckeviciute, J.; Zhang, M.; Whittingham, M. S.; Meng, Y. S.; Van der Ven, A. Narrowing the Gap between Theoretical and Practical Capacities in Li-Ion Layered Oxide Cathode Materials. *Advanced Energy Materials* **2017**, *7* (20), 1602888.